Adaptive Estimation of Play Radii for a Prandtl–Ishlinskii Hysteresis Operator

Mohammad Al Janaideh, *Member, IEEE*, Rui Xu, and Xiaobo Tan, *Fellow, IEEE*

***Abstract*— The Prandtl–Ishlinskii (PI) operator is a mathematical model for hysteresis, and it is comprised of weighted superposition of multiple play (backlash) operators. The PI operator has been widely used in modeling and compensation of hysteresis in smart material actuators, robots, and mechanical systems. The behavior of a PI operator is determined by both the weights and the radii of individual play operators. However, existing modeling work has mostly been focused on the identification of the weight parameters by assuming the play radii to be known. While the latter approach is convenient due to the linear relationship between the operator output and the weight parameters, it often requires a large number of plays with preassigned radii in order to adequately capture the hysteresis in a given application. In this work, for the first time, we propose an adaptive estimation algorithm to identify the play radii of a PI operator, to enable accurate modeling of hysteresis with a small number of plays and, thus, reduce the complexity in control. The major challenge lies in the nonlinear, complex, time-varying relationship between the PI operator output and the play radii. The proposed algorithm utilizes available measurement and information, including the instantaneous slope of the hysteretic input–output graph, to derive a modified estimation error function that is proportional to the parameter error. With a mild condition on the input, we establish the persistent excitation of the resulting regressor vector and the parameter convergence under a gradient algorithm with parameter projection. Both simulation and experimental results are presented to illustrate the proposed approach. In particular, comparison results based on experimental data from a piezoelectric nanopositioner show that, with the proposed method, the resulting PI operator outperforms identified PI operators of larger numbers of plays with preassigned radius values.**

***Index Terms*— Adaptive estimation, hysteresis, piezoelectric actuator, Prandtl–Ishlinskii (PI) operator.**

I. Introduction

HYSTERESIS is a nonlinear phenomenon arising in diverse fields, such as mechanics, biology, electronics, and economics [1]. In particular, hysteresis is ubiquitously exhibited by various smart materials—materials that show inherent coupling between mechanical properties and electrical/magnetic/thermal fields and, thus, can be used as sensors and actuators, such as piezoelectrics, magnetostrictives, and shape memory alloys [2], [3]. For most systems, hysteresis is an undesirable property, and proper modeling is essential to effective mitigation of its impact. Aside from models aiming to capture physics of hysteresis in a particular material or system (e.g., the Jiles–Atherton model for ferromagnetic hysteresis [4]), there have also been a number of phenomenological models introduced for hysteresis, examples of which include the Prandtl–Ishlinskii (PI) operator, the Preisach operator [5]–[7], the Krasnoselskii–Pokrovskii operator [8], the Maxwell-slip model [9], the Duhem model [10], [11], and the Bouc–Wen model [12]. These models have been extensively used in adaptive control [13]–[22] and robust control [23]–[26] of systems with hysteresis. Among these, the classical PI operator and its variants [27], [28] have been particularly popular. For example, they have been used in the modeling of a wide range of motion control systems, as actuated by smart materials (e.g., piezoelectric actuators [29]–[31], magnetostrictive actuators [32], and vanadium dioxide actuators [28]), pneumatic artificial muscles [33], and cable-driven mechanisms [34]. An important reason for the wide adoption of the PI models is that, under mild assumptions, they admit analytical inverses [31], [32], [35], [36], which enables efficient implementation of feedforward inverse compensation to mitigate the hysteresis effect.

A classical PI operator is comprised of weighted superposition of many (or a continuum of) elementary play operators. Each play operator, also known as a backlash, is characterized by a radius or threshold parameter that determines the width of its hysteresis loop. The behavior of a PI operator is determined by both the weights, and the radii of individual play operators. Existing work on the modeling and control of PI operators, however, has largely adopted some predefined play radii [19], based on which the corresponding weights are identified. For example, in [37], estimation of weights of a PI operator was considered with an adaptive variable structure to stabilize a nonlinear dynamic system. An adaptive inverse control technique was proposed to compensate for hysteresis in a piezoceramic actuator [20], where the weights of a PI operator were updated online. With predefined radii, it typically requires a large number of play operators to capture the hysteresis with reasonable accuracy. For example, eight, nine, ten, 15, and 15 elementary operators were used in [20], [22], [31], [38], and [39], respectively. A large number of play operators directly translate into the high computational cost associated with model identification and controller implementation. Motivated by the latter, Zhang *et al.* [28] examined the problem of best approximating a PI operator that has a large number of play operators using one with fewer plays.

Different from all aforementioned work, in this brief, we take a new perspective on the identification of a PI

Manuscript received August 11, 2020; revised October 20, 2020; accepted December 15, 2020. Date of publication January 8, 2021; date of current version October 8, 2021. Manuscript received in final form December 17, 2020. Recommended by Associate Editor S. Pirozzi. *(Corresponding authors: Mohammad Al Janaideh; Xiaobo Tan.)*

Mohammad Al Janaideh is with the Department of Mechanical Engineering, Memorial University, St. John's, NL A1B 3X5, Canada (e-mail: maljanaideh@mun.ca).

Rui Xu was with Jilin University, Changchun 130200, China. He is now with the Changchun Institute of Optics, Fine Mechanics and Physics, Chinese Academy of Sciences, Changchun 130033, China (e-mail: xur@ciomp.ac.cn).

Xiaobo Tan is with the Department of Electrical and Computer Engineering, Michigan State University, East Lansing, MI 48824 USA (e-mail: xbtan@egr.msu.edu).

Color versions of one or more figures in this article are available at https://doi.org/10.1109/TCST.2020.3046019.

Digital Object Identifier 10.1109/TCST.2020.3046019

operator, where the required number of play operators and their associated weights are first determined, and then, the radii of the play operators are estimated. The rationale behind this is to obtain a PI operator with the smallest number of plays for capturing the observed input–output hysteresis behavior, which leads to low complexity for the model and the resulting controller/compensator. In practice, the required number of plays and their associated weights can be estimated by examining the slope profile exhibited by the hysteresis loop, as justified in Section III-A and demonstrated experimentally in Section V. The core contribution of this brief focuses on the second step of the modeling process, estimating the play radii once their weights are identified. Specifically, we take an adaptive estimation approach to facilitate online implementation. There exist two fundamental challenges to the formulated adaptive radius estimation problem. First, the estimation error, which is the error between the predicted output (based on the current parameter estimate) and the actual output, is not linearly related to the error in the radius estimate; indeed, it depends on the operating regimes of both the play operator and the time-dependent estimated play operator. The second (subsequent) challenge is that, with the PI operator being a weighted superposition of multiple play operators, it is impossible to infer the operating regimes of individual plays based on just the output of the PI operator. To address the first challenge, we propose the construction of a modified estimation error, which is linearly proportional to the parameter error, using only information available to the user. To address the second challenge, the instantaneous slope of the input–output graph of the PI operator is used to identify the operating regimes of all plays.

With a mild condition on the input to the PI operator, we show that the associated regressor vector for the modified estimation error is persistently exciting, which guarantees the convergence of the estimates of the play radii to their true values under a classical online estimation algorithm (e.g., the gradient algorithm as adopted in this work). Parameter projection is further introduced to ensure that the estimated parameters follow the right ordering. For ease of presentation, the approach is first elaborated with a PI operator consisting of two plays and then extended to the case of n plays. The efficacy of the proposed approach is supported by both simulation and experimental results. In particular, we demonstrate the identification of numbers and weights of play operators and then the online estimation of play radii using one set of hysteresis data from a piezoelectric nanopositioner. Furthermore, we compare the modeling performance of the resulting PI operator with that of a PI operator identified with the traditional approach (preassigning play radii and estimating play weights) and show that the proposed approach outperforms the traditional approach even when the latter uses more plays.

A preliminary version of this work was presented at the 2019 American Control conference [40]. This brief extends and enhances [40] significantly in a number of ways. First and foremost, the proposed approach is now illustrated and evaluated with experiments, where the comparison with the traditional approach is also provided. Among other things, the experimental work demonstrates the feasibility of quick identification of the number and weights of plays in practice, which supports the key assumption used in the radius estimation problem. Second, while the case of a general $n-$play was briefly mentioned in [40], the detailed algorithm and theory (Proposition 3.2) are presented in this brief. Additional technical results, such as Lemma 3.1 and Lemma 3.2 (which is essential for verifying the input condition for parameter convergence in practice), are developed and presented in this brief. Third, this brief presents a more comprehensive simulation evaluation comparing to [40], which only dealt with simulation with two plays under a sinusoidal input. Finally, the writing has been improved throughout this brief, including adding various technical details and clarifications.

The rest of this brief is organized as follows. The play operator and the PI operator are first reviewed in Section II. In Section III, we formulate the estimation problem and present and analyze the proposed radius estimation algorithm, first illustrated with a two-play PI operator and then generalized to the n-play cases. Simulation and experimental results are presented in Sections IV and V, respectively. Finally, concluding remarks are provided in Section VI.

II. Play and Prandtl-Ishlinskii Operators

The play operator is the basic building block for the construction of a Prandtl-Ishlinskii (PI) operator. For a piecewise monotone input function $v \in C[0, T]$, where $C[0, T]$ is the space of continuous functions in the interval $[0, T]$, and an initial condition $x \in \mathbb{R}$, the output of the play operator with a fixed radius $r \geq 0$, $\Gamma_r[v, x] \in C[0, T]$, can be defined as follows. Let $0 = t_0 < t_1 < \cdots < t_m = T$ be a partition of the interval $[0, T]$ such that v is monotone (nondecreasing or nonincreasing) in each interval $[t_{k-1}, t_k]$, $k = 1, \ldots, m$. Let

$$\Gamma_r[v, x](0) = \max\{v(0) - r, \min\{v(0) + r, x\}\}. \tag{1}$$

Then, for $t \in (t_{k-1}, t_k]$, we define recursively

$$\Gamma_r[v, x](t) = \max\{v(t) - r, \min\{v(t) + r, \Gamma_r[v](t_{k-1})\}\}. \tag{2}$$

For ease of presentation, we write $\Gamma_r[v, x](t)$ as $\Gamma_r[v](t)$ when the initial condition is implicitly understood. The play operator is the Lipschitz continuous in $C[0, T]$ in the sense that

$$|\Gamma_r[v_1](t) - \Gamma_r[v_2](t)| \leq \max_{t \in [0,T]} |v_1(t) - v_2(t)| \tag{3}$$

for all piecewise monotone functions $v_1, v_2 \in C[0, T]$ with the initial condition x for both operators. This enables us to extend the play operator by the density argument to the whole space $C[0, T]$. For a fixed input $v \in C[0, T]$ and time $t \in [0, T]$, when we consider $\Gamma_r[v](t)$ as a function of the radius $r \geq 0$, it is known that it is Lipschitz continuous with the Lipschitz constant 1 [41]. The output of the PI operator consists of a weighted sum

$$y(t) = \sum_{i=1}^{n} p_i \Gamma_{r_i}[v](t) \tag{4}$$

of play operators with radii $r_i \geq 0$, where $r_1 \leq r_2 \leq \cdots \leq r_n$, and weights $p_i > 0$. Since the play operator Γ_r is the Lipschitz continuous with respect to r, it is concluded that

the PI operator is also the Lipschitz continuous with respect to $(r_1, \ldots, r_n)$, for a given input $v(t) \in C[0, T]$. Note that the PI operator is analytically invertible with its inverse represented as another PI operator [42].

In this brief, we consider the radii r_i of the PI operator as unknown variables and aim to estimate them online. Since these estimates are time-dependent, we need to consider play operators and PI operators with time-dependent radii $\hat{r}_i(t)$. The output of a play operator with the estimated radius $\hat{r}(t) \geq 0$, for $t \in (t_{k-1}, t_k]$, is expressed as

$$\hat{y}(t) = \max\{v(t) - \hat{r}(t), \min\{v(t) + \hat{r}(t), \hat{m}(t_{k-1})\}\} \quad (5)$$

where

$$\hat{m}(t_{k-1}) = \Gamma_{\hat{r}(t_{k-1})}[v](t_{k-1}) \quad (6)$$

and $\hat{m}(0) = \max\{v(0) - \hat{r}(0), \min\{v(0) + \hat{r}(0), x\}\}$ for the initial condition x. The operator $\Gamma_{\hat{r}(t)}[.]$ is called a time-dependent play, the properties of which can be found in [43].

Similarly, a time-dependent PI operator can be expressed as

$$\hat{y}(t) = \sum_{i=1}^{n} p_i \Gamma_{\hat{r}_i(t)}[v](t). \quad (7)$$

III. Online Estimation of Play Radii

A. Problem Setup

Consider a PI operator of the form (4), where the number of plays, n, and the weights $\{p_i\}_{i=1}^n$ are known. Given the input function $v(t)$ and the corresponding output $y(t)$ of the PI operator, for $t \geq 0$, the goal is to estimate online the radii values $\{r_i\}_{i=1}^n$.

Before presenting the proposed estimation algorithm, we first justify known number and weights, based upon the observation that such information can be readily extracted from the measured hysteresis loop of the PI operator, as summarized in the following lemma and further demonstrated in Section V with experimental results.

Lemma 1: Consider a PI operator in the form of (4), where $0 < r_1 \leq r_2 \leq \cdots \leq r_n$. Then, the segments of any hysteresis loop of the PI operator can take up to $n+1$ different values of slope, $\sum_{j=1}^{i-1} p_j$, for $i = 1, \ldots, n+1$. Furthermore, if the input v has at least one reversal and spans a range greater than $2r_n$, the corresponding hysteresis graph will show all $n+1$ slope values.

Proof: The slope of the output–input graph of a single (unweighted) play with radius r_i is 1 when the play operates on the lower (respectively, upper) envelope (i.e., the linear boundary $z = v - r_i$ and $z = v + r_i$, respectively) and is 0 when it operates in the interior. For a PI operator with multiple plays, when the input v is increasing, each play operator operates either on the lower envelope or in the interior, and if play i operates on the lower envelope, so is any play j with $j < i$. Conversely, when the input v is decreasing, each play operator operates either on the upper envelope or in the interior, and if play i operates on the upper envelope, so is any play j with $j < i$. From these observations, one can see the possible slope values for the hysteresis graph have to be in the form of $\sum_{j=1}^{i-1} p_j$, for some $i \in \{1, \ldots, n+1\}$. When the input v spans a range larger than $2r_n$ and has at least one reversal, each play has to traverse both an interior operating regime and a linear envelope regime. As a result, all $n+1$ slope values will be exhibited in the output–input hysteresis graph. ■

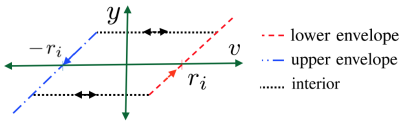

Fig. 1. Output–input graph of a single play with radius r_i, which shows the upper envelope, the lower envelope, and the interior.

Remark 1: It is assumed in Lemma 1 that the smallest radius $r_1 > 0$. If this is not the case (namely, $r_1 = 0$, which means that the PI operator has a linear nonhysteretic element), Lemma 1 holds true except that there will be n distinct slope values, taking the form of $\sum_{j=1}^{i} p_j$, $i = 1, \ldots, n$. The main discussion of this brief focuses on the scenario where the smallest radius is positive (instead of zero). If the smallest radius is zero (the nonhysteretic play has a positive weight), then the minimal slope displayed by the hysteresis loop is positive and corresponds to the weight of the nonhysteretic play. In that case, one can subtract this value from the output to obtain a "modified output" corresponding to all hysteretic play operators. With the original input but the modified output, the weights of the hysteretic plays can be identified using the algorithm presented in this brief.

Remark 2: From Lemma 1, by inspecting the slope values of the hysteresis graph of the PI operator obtained with an input satisfying the (fairly mild) condition therein, one can infer the number and weights of play operators for the PI operator. Furthermore, the slope value of any hysteresis segment, along with the knowledge of whether v is increasing or decreasing during that segment, uniquely determines the states of all play operators. The latter observation will be used in the development of our estimation algorithm, as elaborated in Section III-B.

B. Radius Estimation for the Two-Play Case

The estimation error for the PI operator is defined as

$$\begin{aligned} e(t) &= \hat{y}(t) - y(t) \\ &= \sum_{i=1}^{n} p_i (\Gamma_{\hat{r}_i(t)}[v](t) - \Gamma_{r_i}[v](t)). \end{aligned} \quad (8)$$

Due to the highly nonlinear relationship between the play output and its radius, the estimation error $e(t)$ is not linear with respect to the parameter errors, $\hat{r}_i(t) - r_i$, which is a major challenge in the parameter estimation. This challenge has been overcome in this work with the introduction of a modified estimation error. To facilitate the discussion, we first illustrate the approach with the special case of two play operators, before presenting the results on the general case of n plays.

1) Modified Estimation Error: We enumerate all possible configurations of the operating regimes for the four play operators involved: Γ_{r_1}, Γ_{r_2}, $\Gamma_{\hat{r}_1(t)}$, and $\Gamma_{\hat{r}_2(t)}$. Fig. 1 illustrates the three operating regimes of the play operator. First, consider the case when v is increasing. There are three possibilities for just the combination of Γ_{r_1} and Γ_{r_2}: 1) Γ_{r_2} is on its lower

envelope, in which case Γ_{r_1} has to be on its lower envelope as well (since $r_1 \leq r_2$); 2) Γ_{r_2} is in its interior, and Γ_{r_1} is on its lower envelope; and 3) both Γ_{r_1} and Γ_{r_2} are in their interiors. Similarly, for each of these three cases, there are three subcases for the combination of $\Gamma_{\hat{r}_1(t)}$ and $\Gamma_{\hat{r}_2(t)}$. This results in nine subcases when v is increasing. Likewise, there are nine subcases when v is decreasing, leading to a total of 18 subcases.

As will be illustrated in the following, in each of the subcases, we use the sign of input change, the instantaneous slope $\eta(t)$ for the PI operator and the information from the estimator to uniquely decide the operating regimes of the two original plays and two estimated plays. Correspondingly, one can construct a suitable modified estimation error $e_\delta(t)$ based on the original estimation error $e(t)$, where $e_\delta(t)$ is proportional to the parameter error $\{\tilde{r}_i(t)\}$, where $\tilde{r}_i(t) = r_i - \hat{r}_i(t)$. We now illustrate the three subcases under Case I (increasing v with both plays operating on lower envelopes): $v(t) > v(t_{k-1})$, $y(t) > y(t_{k-1})$, output–input slope $\eta = p_1 + p_2$, and $y(t) = p_1(v(t) - r_1) + p_2(v(t) - r_2)$. Denote $\Delta v(t) = v(t) - v(t_k)$.

1) *Case I-1:* Both estimated plays are in interiors. In this case, $\hat{y}(t) = p_1(v(t_{k-1}) + \hat{r}_1(t_{k-1})) + p_2(v(t_{k-1}) + \hat{r}_2(t_{k-1}))$, and $e(t) = p_1(-\Delta v(t) + \hat{r}_1(t_{k-1}) + r_1) + p_2(-\Delta v(t) + \hat{r}_2(t_{k-1}) + r_2)$. Then, we add $-\hat{r}_1(t) + \hat{r}_1(t)$ and $-\hat{r}_2(t) + \hat{r}_2(t)$ to the terms in $e(t)$ associated with p_1 and p_2, respectively, and arrive at

$$\begin{aligned} e(t) = {} & p_1(-\Delta v(t) + \hat{r}_1(t_{k-1}) + \tilde{r}_1(t) + \hat{r}_1(t)) \\ & + p_2(-\Delta v(t) + \hat{r}_2(t_{k-1}) + \tilde{r}_2(t) + \hat{r}_2(t)) \end{aligned} \tag{9}$$

$$\begin{aligned} e(t) = {} & p_1(\tilde{r}_1(t)) + p_1(-\Delta v(t) + \hat{r}_1(t_{k-1}) + \hat{r}_1(t)) \\ & + p_2(\tilde{r}_2(t)) + p_2(-\Delta v(t) + \hat{r}_2(t_{k-1}) + \hat{r}_2(t)). \end{aligned} \tag{10}$$

Then, by defining (all information needed is available to the user) $\delta_1(t) = p_1(-\Delta v(t) + \hat{r}_1(t_{k-1}) + \hat{r}_1(t)) + p_2(-\Delta v(t) + \hat{r}_2(t_{k-1}) + \hat{r}_2(t))$ and subtracting it from $e(t)$, one can obtain a modified estimation error e_δ

$$e_\delta(t) = e(t) - \delta_1(t) \tag{11}$$

$$= p_1\tilde{r}_1(t) + p_2\tilde{r}_2(t). \tag{12}$$

2) *Case I-2:* $\Gamma_{\hat{r}_1(t)}$ is on its lower envelope, and $\Gamma_{\hat{r}_2(t)}$ is in its interior. In this case, $\hat{y}(t) = p_1(v(t) - \hat{r}_1(t)) + p_2(v(t_{k-1}) + \hat{r}_2(t_{k-1}))$, and $e(t) = p_1(r_1 - \hat{r}_1(t)) + p_2(\hat{r}_2(t_{k-1}) + r_2 - \Delta v(t))$. We follow similar steps as in Case I-1 and define $\delta_2(t) = p_2(-\Delta v(t) + \hat{r}_2(t_{k-1}) + \hat{r}_2(t))$, which can be used to define a modified estimation error e_δ:

$$\begin{aligned} e_\delta(t) &= e(t) - \delta_2(t) \\ &= p_1\tilde{r}_1(t) + p_2\tilde{r}_2(t). \end{aligned} \tag{13}$$

3) *Case I-3:* Both estimated plays are on their lower envelopes. In this case, $\hat{y}(t) = p_1(v(t) - \hat{r}_1(t)) + p_2(v(t) - \hat{r}_2(t))$ and $e(t) = p_1(r_1 - \hat{r}_1(t)) + p_2(r_2 - \hat{r}_2(t))$, which is already in a desired form. With $\delta_3(t) = 0$, one can obtain a modified estimation error e_δ

$$\begin{aligned} e_\delta(t) &= e(t) - \delta_3(t) \\ &= p_1\tilde{r}_1(t) + p_2\tilde{r}_2(t). \end{aligned} \tag{14}$$

It can be observed that, for all three subcases under Case I, the modified error takes the same form, as shown in (12)–(14). Similarly, for Case II, one can construct the modified estimation error function that is represented as

$$e_\delta(t) = p_1\tilde{r}_1(t) - p_2\tilde{r}_2(t) \tag{15}$$

and for Case III

$$e_\delta(t) = -p_1\tilde{r}_1(t) - p_2\tilde{r}_2(t). \tag{16}$$

Likewise, one can perform similar manipulations when v is decreasing, where three principal cases are: (IV) both plays are on their upper envelopes; (V) Γ_{r_2} is in its interior, and Γ_{r_1} is on its upper envelope; and (VI) both Γ_{r_2} and Γ_{r_1} are in their interiors. The modified estimation error for all six principal cases (I–VI) can be summarized as

$$e_\delta(t) = \begin{cases} (p_1\tilde{r}_1(t) + p_2\tilde{r}_2(t))\text{sgn}(\Delta v(t)), & \text{Cases I\& IV} \\ (p_1\tilde{r}_1(t) - p_2\tilde{r}_2(t))\text{sgn}(\Delta v(t)), & \text{Cases II\& V} \\ (-p_1\tilde{r}_1(t) - p_2\tilde{r}_1(t))\text{sgn}(\Delta v(t)), & \text{Cases III\& VI} \end{cases} \tag{17}$$

where $\text{sgn}(\Delta v(t)) = 1$ for $\Delta v(t) > 0$ and $\text{sgn}(\Delta v(t)) = -1$ for $\Delta v(t) < 0$. We note that, $e_\delta(t)$, as calculated by subtracting proper $\delta_i(t)$ function from $e(t)$ [e.g., as in (11)], will be used in the execution of the adaptive estimation algorithm. On the other hand, (17) is used to linearly correlate the modified estimation error with the parameter errors, $\tilde{r}_1(t)$ and $\tilde{r}_2(t)$, which will be instrumental in the convergence analysis of the algorithm (in particular, in the proof of Proposition 3.1 later). Define $\mathbf{p} = (p_1, p_2)^T$, $\mathbf{r} = (r_1, r_2)^T$, $\hat{\mathbf{r}} = (\hat{r}_1, \hat{r}_2)^T$, and $\tilde{\mathbf{r}} = (\tilde{r}_1, \tilde{r}_2)^T$. We can rewrite (17) as

$$e_\delta(t) = \text{sgn}(\Delta v(t))\phi^T(t)\tilde{\mathbf{r}}(t) \tag{18}$$

where

$$\phi(t) = \begin{cases} (p_1, p_2)^T, & \text{Cases I \& IV} \\ (p_1, -p_2)^T, & \text{Cases II \& V} \\ (-p_1, -p_2)^T, & \text{Cases III \& VI.} \end{cases} \tag{19}$$

2) Adaptive Estimation Law for the Case of Two Plays: With a (modified) estimation error in the form of (18), one can employ a number of classical algorithms to estimate the parameter $\mathbf{r}$ (see [44]). Here, we proceed with the gradient algorithm with parameter projection. Define the cost function as

$$J(\tilde{\mathbf{r}}(t)) = \frac{e_\delta^2(t)}{2}. \tag{20}$$

The parameter estimate $\hat{\mathbf{r}}$ needs to satisfy the following constraints: $\hat{r}_2 \geq \hat{r}_1 \geq 0$. To facilitate that, we define two constraint sets, the intersection of which defines the feasible set for the parameter estimate:

$$\Omega_1 = \{(\hat{r}_1, \hat{r}_2) \in \mathbb{R}^2 | g_1(\hat{r}_1, \hat{r}_2) = -\hat{r}_1 \leq 0\}$$
$$\Omega_2 = \{(\hat{r}_1, \hat{r}_2) \in \mathbb{R}^2 | g_2(\hat{r}_1, \hat{r}_2) = \hat{r}_1 - \hat{r}_2 \leq 0\}.$$

Then, the boundaries are

$$\delta\Omega_1 = \{(\hat{r}_1, \hat{r}_2) \in \mathbb{R}^2 | g_1(\hat{r}_1, \hat{r}_2) = 0\}$$
$$\delta\Omega_2 = \{(\hat{r}_1, \hat{r}_2) \in \mathbb{R}^2 | g_2(\hat{r}_1, \hat{r}_2) = 0\}.$$

The interiors of the sets are denoted as

$$\Omega_1^0 = \{(\hat{r}_1, \hat{r}_2) \in \mathbb{R}^2 | g_1(\hat{r}_1, \hat{r}_2) < 0\}$$
$$\Omega_2^0 = \{(\hat{r}_1, \hat{r}_2) \in \mathbb{R}^2 | g_2(\hat{r}_1, \hat{r}_2) < 0\}.$$

The gradient algorithm with parameter projection [44] can then be expressed as

$$\dot{\hat{\mathbf{r}}} = \begin{cases} \Lambda \text{sgn}(\Delta v(t)) e_\delta \phi, & \textbf{if} \begin{cases} \textbf{(a)}\ \hat{\mathbf{r}} \in \Omega_1^0 \cap \Omega_2^0 \\ \text{or} \\ \textbf{(b)}\ \hat{\mathbf{r}} \in \delta\Omega_i, \hat{\mathbf{r}} \notin \delta\Omega_{3-i}, \text{and} \\ (\Lambda \text{sgn}(\Delta v(t) e_\delta \phi)^T \nabla g_i \le 0) \\ \text{for } i = 1 \text{ or } i = 2 \\ \text{or} \\ \textbf{(c)}\ \hat{\mathbf{r}} \in \delta\Omega_1 \cap \Omega_2 \text{ and} \\ (\Lambda \text{sgn}(\Delta v(t)) e_\delta \phi)^T \nabla g_i \le 0 \\ \text{for both } i = 1 \text{ and } 2 \end{cases} \\ \Lambda \text{sgn}(\Delta v(t)) e_\delta \phi - \dfrac{\nabla g_1 \nabla g_1{}^T}{\nabla g_1^T \nabla g_1} \Lambda \text{sgn}(\Delta v(t)) e_\delta \phi \\ \quad \textbf{if } \hat{\mathbf{r}} \in \delta\Omega_i,\ \hat{\mathbf{r}} \notin \delta\Omega_{3-i}, \text{ and} \\ \quad (\Lambda \text{sgn}(\Delta v(t)) e_\delta \phi)^T \nabla g_i > 0 \\ \quad \text{for } i = 1 \text{ or } i = 2 \\ 0 \quad \textbf{if otherwise} \end{cases} \tag{21}$$

where

$$\Lambda = \begin{bmatrix} \gamma_1 & 0 \\ 0 & \gamma_2 \end{bmatrix} > 0$$

represents the adaptation gains, and ∇g_1 and ∇g_2 represent the gradients of g_1 and g_2, respectively.

3) Parameter Convergence Analysis:

Proposition 1: Assume the input v to be periodic with a spanned range larger than $2r_2$. The estimation algorithm (21) will result in exponential convergence of $\hat{\mathbf{r}}(t)$ to $\mathbf{r}$ as $t \to \infty$.

Proof: For the convenience of discussion, we consider the gradient law without parameter projection (parameter projection only helps convergence; see [44]). From (18) and (21), it can be readily derived that

$$\dot{\tilde{\mathbf{r}}} = -\Lambda \phi(t) \phi(t)^T \tilde{\mathbf{r}}(t) \tag{22}$$

where $\phi(t)$ is governed by (19). With the assumption on v, the PI operator will traverse all six principal cases of configurations (I–VI) during each period T. From (19), the regressor vector ϕ will rotate between linearly independent vectors $(p_1, p_2)^T$ and $(p_1, -p_2)^T$ periodically, with which one can conveniently establish that $\phi(t)$ is persistently exciting. The exponential convergence of $\tilde{\mathbf{r}} \to 0$ then follows [44]. ■

C. Radius Estimation for the General n-Play Case

The algorithm and analysis in Section III-B can be readily extended to a general PI operator consisting of n play operators. In particular, for an increasing input v, one can enumerate $n+1$ principal cases based on the configuration of the operating regimes of all play operators. For each principal case, one can enumerate $n+1$ subcases covering all possible configurations of the operating regimes of the estimated play operators. The beauty is that, for a given principal case, the modified estimation error e_δ can be expressed as $e_\delta(t) = \phi^T(t)\tilde{\mathbf{r}}(t)$ for all its subcases with the same expression for $\phi(t)$, as illustrated for the two-play case in Section III. The analogous observation holds true for a decreasing v. Specifically, for an increasing v, the $n+1$ principal cases correspond to the slope η value of 0, p_1, p_1+p_2, …, $p_1+p_2+\cdots+p_n$. In shorthand, for $i = 1, \ldots, n+1$, the slope of the principal case i is $\sum_{j=1}^{i-1} p_j$. The regressor vector ϕ for case i (for all its $(n+1)$ subcases) satisfies: $\phi_j = \text{sgn}(i-j)p_j$, where ϕ_j denotes the jth element of ϕ, and here, we take convention $\text{sgn}(0) = -1$.

One can see, again, in the $n-$play case, that the regressor vector ϕ will rotate between vectors that encompass n linearly independent vectors: $(p_1, p_2, \ldots, p_{n-1}, p_n)^T$, $(p_1, p_2, \ldots, p_{n-1}, -p_n)^T$,…, $(p_1, -p_2, \ldots, -p_{n-1}, -p_n)^T$, and therefore, it will be persistently exciting under a similar assumption used in Lemma 1, where the range of the input v is required to be larger than $2\ r_n$, with r_n being the largest play radius. One can then employ the gradient algorithm with parameter projection, as summarized in the following.

The parameter estimate $\hat{\mathbf{r}}$ needs to satisfy the following constraints: $\hat{r}_n \ge \cdots \ge \hat{r}_2 \ge \hat{r}_1 \ge 0$. To facilitate that, we define n constraint sets, the intersection of which defines the feasible set for the parameter estimate

$$\Omega_1 = \{(\hat{r}_1, \hat{r}_2, \ldots, \hat{r}_n,) \in \mathbb{R}^n | g_1(\hat{r}_1, \hat{r}_2, \ldots, \hat{r}_n) = -\hat{r}_1 \le 0\}$$
$$\Omega_2 = \{(\hat{r}_1, \hat{r}_2, \ldots, \hat{r}_n) \in \mathbb{R}^n | g_2(\hat{r}_1, \hat{r}_2, \ldots, \hat{r}_n) = \hat{r}_1 - \hat{r}_2 \le 0\}$$
$$\vdots$$
$$\Omega_n = \{(\hat{r}_1, \hat{r}_2, \ldots, \hat{r}_n) \in \mathbb{R}^n | g_n(\hat{r}_1, \hat{r}_2, \ldots, \hat{r}_n) = \hat{r}_{n-1} - \hat{r}_n \le 0\}.$$

Then, the boundaries of these constraint sets are

$$\delta\Omega_1 = \{(\hat{r}_1, \hat{r}_2, \ldots, \hat{r}_n) \in \mathbb{R}^n | g_1(\hat{r}_1, \hat{r}_2, \ldots, \hat{r}_n) = 0\}$$
$$\delta\Omega_2 = \{(\hat{r}_1, \hat{r}_2, \ldots, \hat{r}_n)) \in \mathbb{R}^n | g_2(\hat{r}_1, \hat{r}_2, \ldots, \hat{r}_n) = 0\}$$
$$\vdots$$
$$\delta\Omega_n = \{(\hat{r}_1, \hat{r}_2, \ldots, \hat{r}_n) \in \mathbb{R}^n | g_n(\hat{r}_1, \hat{r}_2, \ldots, \hat{r}_n) = 0\}.$$

The interiors of the constraint sets are

$$\Omega_1^0 = \{(\hat{r}_1, \hat{r}_2, \ldots, \hat{r}_n) \in \mathbb{R}^n | g_1(\hat{r}_1, \hat{r}_2, \ldots, \hat{r}_n) < 0\}$$
$$\Omega_2^0 = \{(\hat{r}_1, \hat{r}_2, \ldots, \hat{r}_n) \in \mathbb{R}^n | g_2(\hat{r}_1, \hat{r}_2, \ldots, \hat{r}_n) < 0\}$$
$$\vdots$$
$$\Omega_n^0 = \{(\hat{r}_1, \hat{r}_2, \ldots, \hat{r}_n) \in \mathbb{R}^n | g_n(\hat{r}_1, \hat{r}_2, \ldots, \hat{r}_n) < 0\}.$$

Then, the estimation algorithm can be presented as

$$\dot{\hat{\mathbf{r}}} = \begin{cases} \Lambda \text{sgn}(\Delta v(t)) e_\delta \phi, \textbf{ if } \begin{cases} \textbf{(a)}\ \hat{\mathbf{r}} \in \bigcap_{i=1}^{n} \Omega_i^0 \\ \text{or} \\ \textbf{(b)}\ \hat{\mathbf{r}} \in \delta\Omega_i, \hat{\mathbf{r}} \notin \delta\Omega_j, \text{ for } j \neq i \\ \text{and} \\ (\Lambda \text{sgn}(\Delta v(t) e_\delta \phi)^T \nabla g_i \leq 0 \\ \text{for } i = 1, 2, \ldots \text{or } n \\ \text{or} \\ \textbf{(c)} \text{ for some } k \in \{1, \ldots, n\} \\ \hat{\mathbf{r}} \in \bigcap_{j=1}^{k} \delta\Omega_{i_j}, \text{ and} \\ (\Lambda \text{sgn}(\Delta v(t)) e_\delta \phi)^T \nabla g_{i_j} < 0 \\ \text{for all } i_j, \text{ where } i_1, \ldots, i_k \\ \text{are distinct elements for} \\ \{1, \ldots, n\} \end{cases} \\ \Lambda \text{sgn}(\Delta v(t)) e_\delta \phi - \dfrac{\nabla g_i \nabla g_i^T}{\nabla g_i^T \nabla g_i} \Lambda \text{sgn}(\Delta v(t)) e_\delta \phi \\ \quad \textbf{if } \hat{\mathbf{r}} \in \delta\Omega_i, \ \hat{\mathbf{r}} \notin \delta\Omega_j, \text{ for } j \neq i \\ \quad \text{and } \left(\Lambda \text{sgn}\left(\Delta v(t)\right) e_\delta \phi\right)^T \nabla g_i > 0 \\ \quad \text{for some } i \in \{1, \ldots, n\} \\ 0, \textbf{ if otherwise} \end{cases} \tag{23}$$

where $\Lambda > 0$ represents the adaptation gains, and ∇g_i represents the gradient of g_i.

We summarize the above discussions in the following proposition.

Proposition 2: For a PI operator with n plays, assume the input v to be periodic with a spanned range larger than $2r_n$. The estimation algorithm (23) will result in exponential convergence of $\hat{\mathbf{r}}(t)$ to $\mathbf{r}$ as $t \to \infty$.

Remark 3: The requirement of periodic v in Proposition 2 can be relaxed to the following: the rate of change for v is bounded, and there exists $T > 0$ such that, for any time interval $[t_0, t_0 + T]$, v has at least one reversal and spans a range larger than $2r_n$.

Proposition 2 requires the range of the input v to be larger than twice of the largest play radius r_n; however, the value of r_n is not known in advance. The following lemma provides a practical means for obtaining a lower bound for 2 r_n and, thus, for checking a necessary condition v that needs to be satisfied, i.e., the range of v should be not be smaller than the width ρ of the observed hysteresis loop. In addition, it provides an upper bound and sufficient condition for 2 r_n in terms of ρ and play weights. For a hysteresis loop, we define its width as the largest separation between two input values that correspond to the same output value.

Lemma 2: For a PI operator with n plays satisfying the condition in Lemma 1, the maximum width of its hysteresis loop generated among all possible inputs is

$$\rho = 2\frac{\sum_{i=1}^{n} p_i r_i}{\sum_{i=1}^{n} p_i} \tag{24}$$

$$2r_1 \leq \rho \leq 2r_n \tag{25}$$

$$2r_n < \frac{\sum_{i=1}^{n} p_i}{p_n} \rho. \tag{26}$$

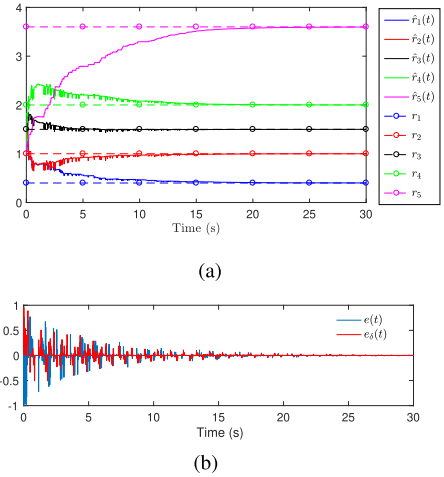

Fig. 2. Simulation results for the case of a PI operator with five plays with unknown radii of $r_1 = 0.4$, $r_2 = 1$, $r_3 = 1$, $r_4 = 2$, and $r_5 = 3.6$: (a) estimated radii $\hat{r}_1(t)$, $\hat{r}_2(t)$, $\hat{r}_3(t)$, $\hat{r}_4(t)$, and $\hat{r}_5(t)$ and (b) time trajectories of the estimation error $e(t)$ and the modified error $e_\delta(t)$.

Proof: For a PI operator, the maximum width of the hysteresis loop is the separation between the increasing and decreasing curves when the plays are on their lower and upper envelopes, respectively. For the increasing curve, the output of PI operator can be expressed as $y(t) = \sum_{i=1}^{n} p_i(v(t) - r_i)$; for the decreasing curve, the output can be expressed as $y(t) = \sum_{i=1}^{n} p_i(v(t) + r_i)$. To figure out the "horizontal" separation between these two curves, without the loss of generality, we can find the input values, v^{*+} and v^{*-}, for both curves, with their corresponding outputs $y(t) = 0$. It can be readily verified the hysteresis loop width $\rho = v^{*+} - v^{*-} = 2(\sum_{i=1}^{n} p_i r_i)/(\sum_{i=1}^{n} p_i)$. Equation (25) is then obtained from (24) by noting $r_1 \leq r_i \leq r_n$, for $i = 1, \ldots, n$. Likewise, (26) is obtained from (24) by noting $p_n r_n < \sum_{i=1}^{n} p_i r_i$. ■

IV. Simulation Results

We perform simulation with the proposed algorithm for the case of a PI operator with a harmonic input of $v(t) = 30 \sin(\omega t)$, where $\omega = 2\pi$ rad/second, five plays with weights of $p_1 = 0.3$, $p_2 = 0.5$, $p_3 = 0.8$, $p_4 = 0.3$, and $p_5 = 0.2$ and unknown radii of $r_1 = 0.4$, $r_2 = 1$, $r_3 = 1.5$, $r_4 = 2$, and $r_5 = 3.6$. The adaption gains are $\gamma_1 = \gamma_2 = \gamma_3 = \gamma_4 = \gamma_5 = 10$. We consider white noise of signal-to-noise ratio (SNR) of 10 dB with the output of the PI operator. Fig. 2 shows the simulation results, where Fig. 2(a) shows the time history of the estimated radii $\hat{r}_1(t)$, $\hat{r}_2(t)$, $\hat{r}_3(t)$, $\hat{r}_4(t)$, and $\hat{r}_5(t)$, and Fig. 2(b) shows the time history of the estimation error $e(t)$ and the modified estimation error $e_\delta(t)$. To show that the algorithm can be used to identify radii with different input signals, we consider a periodic, biased stair-step input shown in Fig. 3(b) with white noise of SNR ratio of 20 dB added to the output of the PI operator. Fig. 3(a) shows the time history of the estimated radii $\hat{r}_1(t)$, $\hat{r}_2(t)$, $\hat{r}_3(t)$, $\hat{r}_4(t)$, and $\hat{r}_5(t)$. To identify the radii with this input, we select the adaption gains as $\gamma_1 = \gamma_2 = \gamma_3 = \gamma_4 = \gamma_5 = 10$. From Fig. 3(a) and (c), it is evident that the proposed algorithm is able to drive the radius estimates to their true values.

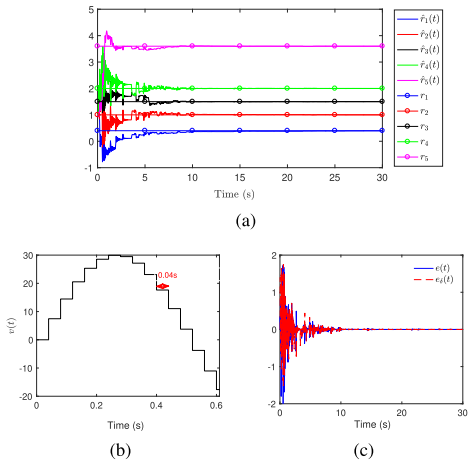

Fig. 3. (a) Simulation results the PI operator with five unknown radii of Fig. 3 with a periodic, biased stair-step input, (b) sample of the biased stair-step input, and (c) time histories of the estimation error $e(t)$ and the modified error $e_\delta(t)$.

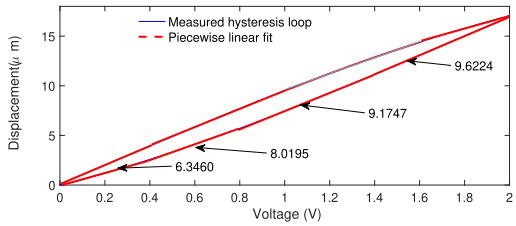

Fig. 4. Voltage-to-displacement major hysteresis loop of the piezo-actuated nanopositioning system and the four identified slopes (piecewise linear fit).

V. Experimental Results

In this section, we present experimental validation of the estimation approach using a piezo-actuated nanopositioning stage (Nano-OP65, Mad City Labs Inc.). A PC equipped with a dSPACE system (RT1104, dSPACE) is used to generate the voltage input signals and to acquire the displacement data from the nanopositioning stage. The voltage input signal is first sent to a power amplifier (Nano Drive, Md City Labs Inc.) with a gain of 15, before being applied to the piezo stage. In this section, we consider the hysteresis loops between the input voltage that is applied to the power amplifier and the measured displacement output.

A. Identification of Number and Weights of Plays

We apply a 1-Hz triangular input voltage of amplitude 2 V to the piezo-actuated nanopositioning system. The measured voltage-to-displacement hysteresis loop is presented in Fig. 4. From the hysteresis loop, we determine that four linear segments suffice to capture the ascending and descending branches. At first, we divide the increasing hysteresis curve into four parts based on the visually observed slope trend. Next, we aim to identify the best slopes that approximate the four segments. In particular, we seek the best match of each segment to a linear function, using a bat-inspired optimization algorithm [45]. The resulting slopes are $s_1 = 6.3460$, $s_2 = 8.0195$, $s_3 = 9.1747$, and $s_4 = 9.6224$. Once the slopes are found, we calculate the play weights based on the relationship between the weights and the slopes as captured in Lemma 3.1: $p_1 = s_1$, $p_2 = s_2 - s_1$, $p_3 = s_3 - s_2$, and $p_4 = s_4 - s_3$, resulting in $p_1 = 6.3460$, $p_2 = 1.6735$, $p_3 = 1.1552$, and $p_4 = 0.4477$.

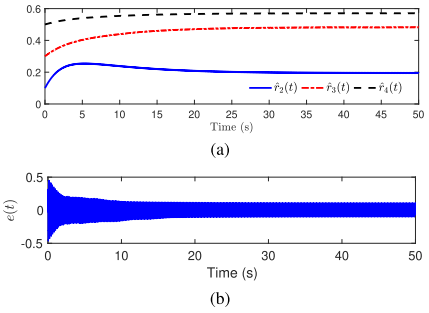

Fig. 5. (a) Estimated radii $\hat{r}_2(t)$, $\hat{r}_3(t)$, and $\hat{r}_4(t)$ based on the measured hysteresis loop in Fig. 4. (b) Estimation error $e(t)$.

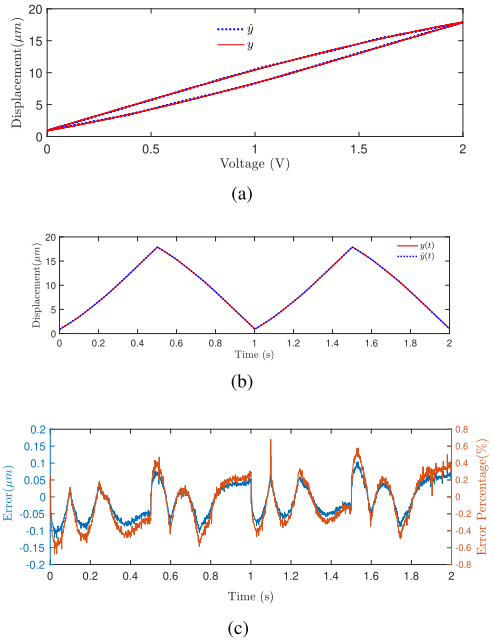

Fig. 6. Modeling performance of the estimated PI operator: (a) comparison between the measured and predicted hysteresis loops. (b) Measured displacement and predicted displacement in time and (c) modeling error $y(t) - \hat{y}(t)$ and the percentage error $(y(t) - \hat{y}(t))/(\max\{y(t)\} - \min\{y(t)\}) \times 100\%$.

The four slopes of the increasing curve are shown in Fig. 4. Since the smallest slope is positive, we infer (see Remark 1) that there is a linear (nonhysteretic) play $r_1 = 0$ with weight p_1. We need to estimate three thresholds $\hat{r}_2(t)$, $\hat{r}_3(t)$, and $\hat{r}_4(t)$.

B. Estimation of Play Radii With the Proposed Algorithm

Based on the data for the major hysteresis loop, we implement the proposed algorithm to estimate the radius values for the four play operators. We use adaption gains of $\gamma_1 = \gamma_2 = \gamma_3 = 20$. Fig. 5 shows the evolution of the parameter estimates and the estimation error. The radius estimates are obtained as $\hat{r}_2 = 0.1945$, $\hat{r}_3 = 0.4826$, and $\hat{r}_4 = 0.5707$. Fig. 6 shows the modeling performance of the resulting PI operator, by comparing the prediction from the identified PI operator with the measurement obtained using the triangular input. In particular, Fig. 6(a) shows the comparison of the hysteresis loops, while Fig. 6(b) compares the predicted output with the measured output in time, and Fig. 6(c) shows the output prediction error, which is less than 0.122 μm for the total displacement range of 17.03 μm.

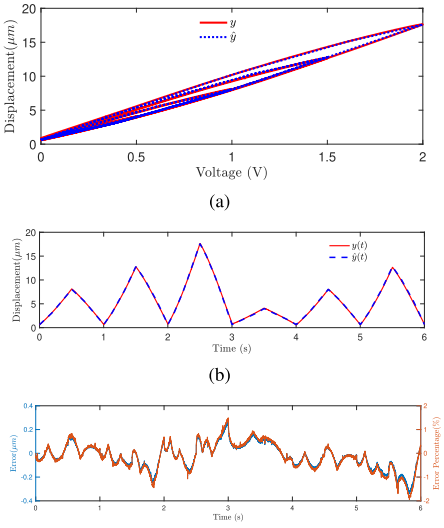

Fig. 7. Validation of the estimated model with a new input that generates both major and minor loops. (a) Comparison between the measured and predicted major and predicted hysteresis loops. (b) Measured displacement and predicted displacement in time and (c) modeling error $y(t) - \hat{y}(t)$ and the percentage error $(y(t) - \hat{y}(t))/(\max\{y(t)\} - \min\{y(t)\}) \times 100\%$.

We further evaluate the obtained PI operator using a different set of measurement data involving an input function that generates both major and minor loops. The comparison between the model prediction and the measured data is shown in Fig. 7. From the figure, it can be concluded that the PI operator with four plays, identified via only the major hysteresis loop data, is able to capture well the hysteretic behavior under more sophisticated inputs.

C. Comparison With the Conventional Approach

In order to demonstrate the merit of identifying a PI operator based on the estimation of play radii, we compare the proposed approach with the conventional approach, where the weights of the plays are identified with the radii of plays assumed to be known. Here, we use the same major hysteresis loop data in Fig. 4 to identify the play weights. Different numbers of play operators of $n = 4, 5, 6, \ldots, 10$, with preassumed radii of $r_i = (i-1)/(n-1), i = 1, 2, \ldots, n$, are used. For example, for a PI operator of seven ($n = 7$) play operators, the selected radii are $r_1 = 0, r_2 = (1)/(6), r_3 = (2)/(6), r_4 = (3)/(6), r_5 = (4)/(6).r_6 = (5)/(6)$, and $r_7 = 1$. The weights are solved for with the nonlinear least-squares command in MATLAB to obtain the optimal weights. Again, with the example of seven plays, the resulting optimized weights from the optimizer are $p_1 = 5.4194$, $p_2 = 2.2159$, $p_3 = 1.2423$, $p_4 = 0.0852$, $p_5 = 0.3505$, $p_6 = 0.0145$, and $p_7 = 0.0099$. The optimized weights $(p_1, p_2, \ldots, p_n)$ and the corresponding predetermined radii $(r_1, r_2, \ldots, r_n)$ are then used to compute major and minor hysteresis loops.

Fig. 8 shows the comparison for the case of a major hysteresis loop (measured data from Fig. 4). Similarly, Fig. 9 shows the comparison for the case involving both major and minor hysteresis loops (measured data from Fig. 7). It can be seen that, in both cases, the proposed approach outperforms the conventional approach even when the latter uses a larger number of plays. For example, for the case in Fig. 9, the proposed

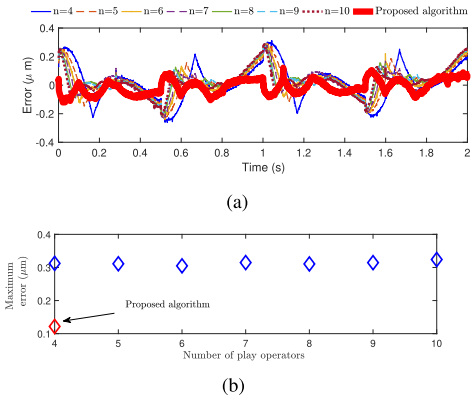

Fig. 8. Comparison of the modeling errors with the proposed and conventional approaches, for the case of a major hysteresis loop: (a) time history of the modeling errors of the conventional approach of n = 4, 5, 6, 7, 8, 9, and 10 and the proposed algorithm with $n = 4$ and (b) resulting maximum modeling error for each case.

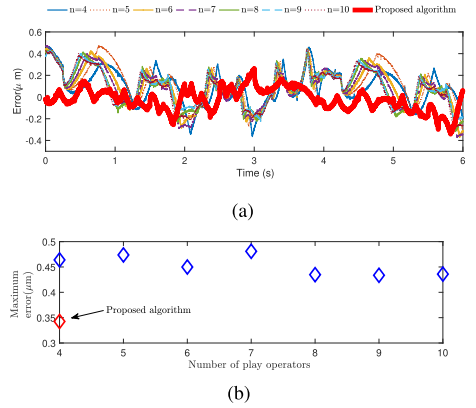

Fig. 9. Modeling errors of the major loop and three minors: (a) time history of the modeling errors of the conventional approach of n = 4, 5, 6, 7, 8, 9, and 10 and the proposed algorithm with $n = 4$ and (b) resulting maximum modeling error for each case.

algorithm ($n = 4$) results in a maximum error of 0.34 μm, while the conventional approach results in a maximum error of 0.48 μm when $n = 7$ and maximum error of 0.44 μm when $n = 10$.

VI. Conclusion

This brief was focused on the identification of the PI operator, which has been used widely to model the hysteresis in smart material-based actuators and other actuation mechanisms. Specifically, we proposed a novel algorithm for the adaptive estimation of play radii, based on the construction of a modified estimation error. With mild conditions on the input, the exponential convergence of parameters was established under the gradient algorithm with parameter projection. The approach was evaluated with both simulation and experimental results. In particular, experimental data from a piezo-based nanopositioning stage were used to illustrate the proposed approach. Furthermore, the comparison with the conventional identification approach for a PI operator shows that the proposed method can better capture the hysteresis behavior even with a smaller number of play operators.

Our future work will be pursued in several directions. First, in this brief, the weights of the plays were identified offline first. It is of interest to explore whether both play weights and

play radii can be jointly estimated online. Second, we plan to extend this work from a classical PI operator to its variants, such as a modified PI operator [27] and a generalized PI operator [28].

REFERENCES

[1] X. Tan and R. Iyer, "Modeling and control of hysteresis: Introduction to the special section," *IEEE Control Syst. Mag.*, vol. 29, no. 1, pp. 26–29, Jan. 2009.

[2] R. Smith, *Smart Material Systems: Model Development*. Philadelphia, PA, USA: SIAM, 2005.

[3] D. Leo, *Engineering Analysis of Smart Material Systems*. Hoboken, NJ, USA: Wiley, 2007.

[4] D. Lederer, H. Igarashi, A. Kost, and T. Honma, "On the parameter identification and application of the jiles-atherton hysteresis model for numerical modelling of measured characteristics," *IEEE Trans. Magn.*, vol. 35, no. 3, pp. 1211–1214, May 1999.

[5] I. D. Mayergoyz, *Mathematical Models of Hysteresis and Their Applications*. New York, NY, USA: Elsevier, 2003.

[6] M. Brokate and J. Sprekels, *Hysteresis and Phase Transitions*. New York, NY, USA: Springer-Verlag, 1996.

[7] X. Tan and J. S. Baras, "Modeling and control of hysteresis in magnetostrictive actuators," *Automatica*, vol. 40, no. 9, pp. 1469–1480, Sep. 2004.

[8] M. A. Krasnosel'skii and A. V. Pokrovskii, *Systems With Hysteresis*. New York, NY, USA: Springer-Verlag, 1989.

[9] Y. Liu, D. Zou, H. Wu, and H. Liu, "Modelling and compensation of hysteresis in piezoelectric actuators based on maxwell approach," *Electron. Lett.*, vol. 52, no. 3, pp. 188–190, Feb. 2016.

[10] R. Ouyang and B. Jayawardhana, "Absolute stability analysis of linear systems with Duhem hysteresis operator," *Automatica*, vol. 50, no. 7, pp. 1860–1866, Jul. 2014.

[11] J. Oh and D. S. Bernstein, "Semilinear Duhem model for rate-independent and rate-dependent hysteresis," *IEEE Trans. Autom. Control*, vol. 50, no. 5, pp. 631–645, May 2005.

[12] F. Ikhouane, V. Mañosa, and J. Rodellar, "Dynamic properties of the hysteretic Bouc-Wen model," *Syst. Control Lett.*, vol. 56, no. 3, pp. 197–205, Mar. 2007.

[13] M. A. Janaideh and D. S. Bernstein, "Adaptive control of uncertain Hammerstein systems with hysteretic nonlinearities," in *Proc. 53rd IEEE Conf. Decis. Control*, Dec. 2014, pp. 545–550.

[14] Ł. Ryba, J. Dokoupil, A. Voda, and G. Besançon, "Adaptive hysteresis compensation on an experimental nanopositioning platform," *Int. J. Control*, vol. 90, no. 4, pp. 765–778, Apr. 2017.

[15] X. Tan and J. S. Baras, "Adaptive identification and control of hysteresis in smart materials," *IEEE Trans. Autom. Control*, vol. 50, no. 6, pp. 827–939, Jun. 2005.

[16] G. Tao and P. V. Kokotović, *Adaptive Control of Systems With Actuator and Sensor Nonlinearities*. Hoboken, NJ, USA: Wiley, 1996.

[17] X. Fan and R. Smith, "Model-based L_1 adaptive control of hysteresis in smart materials," in *Proc. 47th IEEE Conf. Decis. Control*, Dec. 2008, pp. 3251–3256.

[18] X. Chen, T. Hisayama, and C.-Y. Su, "Adaptive control for uncertain continuous-time systems using implicit inversion of Prandtl-Ishlinskii hysteresis representation," *IEEE Trans. Autom. Control*, vol. 55, no. 10, pp. 2357–2363, Oct. 2010.

[19] A. Esbrook, X. Tan, and H. K. Khalil, "Control of systems with hysteresis via servocompensation and its application to nanopositioning," *IEEE Trans. Control Syst. Technol.*, vol. 21, no. 3, pp. 725–738, May 2013.

[20] K. Kuhnen and H. Janocha, "Adaptive inverse control of piezoelectric actuators with hysteresis operators," in *Proc. Eur. Control Conf. (ECC)*, Karlsruhe, Germany, Aug. 1999, pp. 791–796.

[21] A. Esbrook, X. Tan, and H. K. Khalil, "A robust adaptive servocompensator for nanopositioning control," in *Proc. 49th IEEE Conf. Decis. Control (CDC)*, Atlanta, GA, USA, Dec. 2010, pp. 3688–3693.

[22] Y. K. Al-Nadawi, X. Tan, and H. K. Khalil, "An adaptive conditional servocompensator design for nanopositioning control," in *Proc. IEEE 56th Annu. Conf. Decis. Control (CDC)*, Melbourne, VIC, Australia, Dec. 2017, pp. 885–890.

[23] M. Rakotondrabe, K. Rabenorosoa, J. Agnus, and N. Chaillet, "Robust feedforward-feedback control of a nonlinear and oscillating 2-DOF piezocantilever," *IEEE Trans. Autom. Sci. Eng.*, vol. 8, no. 3, pp. 506–519, Jul. 2011.

[24] K. Leang and S. Devasia, "Robust feedforward-feedback control of a nonlinear and oscillating 2-DOF piezocantilever," *IEEE Trans. Control Syst. Technol.*, vol. 15, pp. 927–935, 2007.

[25] B. Jayawardhana, H. Logemann, and E. P. Ryan, "PID control of second-order systems with hysteresis," *Int. J. Control*, vol. 81, no. 8, pp. 1331–1342, Aug. 2008.

[26] J. M. Nealis and R. C. Smith, "Model-based robust control design for magnetostrictive transducers operating in hysteretic and nonlinear regimes," *IEEE Trans. Control Syst. Technol.*, vol. 15, no. 1, pp. 22–39, Jan. 2007.

[27] K. Kuhnen, "Modeling, identification and compensation of complex hysteretic nonlinearities: A modified prandtl-ishlinskii approach," *Eur. J. Control*, vol. 9, no. 4, pp. 407–418, Jan. 2003.

[28] J. Zhang, E. Merced, N. Sepulveda, and X. Tan, "Modeling and inverse compensation of hysteresis in vanadium dioxide using an extended generalized Prandtl-Ishlinskii model," *Smart Mater. Struct.*, vol. 23, pp. 125017-1–125017-10, 2014.

[29] J. Ma, L. Tian, Y. Li, Z. Yang, Y. Cui, and J. Chu, "Hysteresis compensation of piezoelectric deformable mirror based on Prandtl–Ishlinskii model," *Opt. Commun.*, vol. 416, pp. 94–99, Jun. 2018.

[30] F. Stefanski, B. Minorowicz, J. Persson, A. Plummer, and C. Bowen, "Non-linear control of a hydraulic piezo-valve using a generalised Prandtl–Ishlinskii hysteresis model," *Mech. Syst. Signal Process.*, vol. 82, no. 1, pp. 412–431, 2017.

[31] M. Al Janaideh, M. Rakotondrabe, and O. Aljanaideh, "Further results on hysteresis compensation of smart micropositioning systems with the inverse Prandtl–Ishlinskii compensator," *IEEE Trans. Control Syst. Technol.*, vol. 24, no. 2, pp. 428–439, Mar. 2016.

[32] M. Al Janaideh and O. Aljanaideh, "Further results on open-loop compensation of rate-dependent hysteresis in a magnetostrictive actuator with the prandtl-ishlinskii model," *Mech. Syst. Signal Process.*, vol. 104, pp. 835–850, May 2018.

[33] S. Xie, J. Mei, H. Liu, and Y. Wang, "Hysteresis modeling and trajectory tracking control of the pneumatic muscle actuator using modified Prandtl–Ishlinskii model," *Mechanism Mach. Theory*, vol. 120, pp. 213–224, Feb. 2018.

[34] O. Aljanaideh, M. Miyasaka, and B. Hannaford, "Integrated asymmetric stop operator based model for strain stress hysteresis characteristics of cable driven robots loaded longitudinally," in *Proc. Int. Conf. Intell. Robot. Syst.*, Vancouver, BC, Canada, 2017, pp. 2543–2548.

[35] M. Al Janaideh, C.-Y. Su, and S. Rakheja, "Inverse compensation error of the prandtl-ishlinskii model," in *Proc. IEEE 51st IEEE Conf. Decision Control (CDC)*, Maui, HI, USA, Dec. 2012, pp. 1597–1602.

[36] P. Krejí, M. Al Janaideh, and F. Deasy, "Inversion of hysteresis and creep operators," *Phys. B, Condens. Matter*, vol. 407, no. 9, pp. 1354–1356, May 2012.

[37] C.-Y. Su, Q. Wang, X. Chen, and S. Rakheja, "Adaptive variable structure control of a class of nonlinear systems with unknown Prandtl-Ishlinskii hysteresis," *IEEE Trans. Autom. Control*, vol. 50, no. 12, pp. 2069–2074, Dec. 2005.

[38] W. T. Ang, P. K. Khosla, and C. N. Riviere, "Feedforward controller with inverse rate-dependent model for piezoelectric actuators in trajectory-tracking applications," *IEEE/ASME Trans. Mechatronics*, vol. 12, no. 2, pp. 134–142, Apr. 2007.

[39] M. Rakotondrabe, "Multivariable classical Prandtl–Ishlinskii hysteresis modeling and compensation and sensorless control of a nonlinear 2-dof piezoactuator," *Nonlinear Dyn.*, vol. 89, no. 1, pp. 481–499, Jul. 2017.

[40] M. Al Janaideh and X. Tan, "Adaptive estimation of threshold parameters for a Prandtl-Ishlinskii hysteresis operator," in *Proc. Amer. Control Conf.*, Philadelphia, PA, USA, 2019, pp. 3770–3775.

[41] P. Krejci, *Hysteresis, Convexity and Dissipation in Hyperbolic Equations* (GAKUTO International Series. Mathematical Sciences and Applications), vol. 8. Gakkotosho, Tokyo, 1996.

[42] P. Krejci and K. Kuhnen, "Inverse control of systems with hysteresis and creep," *IEE Proc. Control Theory Appl.*, vol. 148, no. 3, pp. 185–192, May 2001.

[43] M. Al Janaideh and P. Krejí, "An inversion formula for a Prandtl–Ishlinskii operator with time dependent thresholds," *Phys. B, Condens. Matter*, vol. 406, no. 8, pp. 1528–1532, Apr. 2011.

[44] P. A. Ioannou and J. Sun, *Robust Adaptive Control*. Upper Saddle River, NJ, USA: Prentice-Hall, 1995.

[45] X. S. Yang, "Bat algorithm for multi-objective optimisation," *Int. J. Bio-Inspired Comput.*, vol. 3, no. 5, pp. 267–274, 2012.